Unusually high selectivity to C_{2+} alcohols on bimetallic CoFe catalysts during CO hydrogenation

V.A. de la Peña O'Shea[a], N.N. Menéndez[b], J.D. Tornero[b], and J.L.G. Fierro[a,*]

[a]*Instituto de Catálisis y petroleoquímica, CSIC, Cantoblanco, 28049 Madrid, Spain; http://www.icp.csic.es/eac/index.htm*
[b]*Universidad Autónoma de Madrid, Cantoblanco, 28049 Madrid, Spain*

Received 11 March, 2003; accepted 13 March 2003

Silica-supported cobalt and iron catalysts (10% Co and 5% or 1% Fe) were prepared and tested in a flow reactor in the hydrogenation of CO, using $H_2/CO = 2:1$ (molar) ratio in the feed, an overall pressure of 20 bar, and temperatures of 493, 513 and 533 K. Activity and product distribution were found to depend strongly on the composition of the catalysts. Thus, the Fe-free catalyst was selective toward C_{5+} formation (67% selectivity to C_{5+}) and a low methanation rate, while the Co-free counterpart was less selective toward C_{5+}, with a simultaneous increase in the formation of lighter fractions and alcohols. The behavior of the bimetallic CoFe catalysts was different. In the bimetallic CoFe10/5-c catalyst, selectivity to alcohols increased with respect to the monometallic Co10-c, and this was moderately high (15% to C_{3+}OH alcohols). In the bimetallic CoFe10/1-c sample, selectivity to alcohols was fairly high (29%), and ethanol reached the highest proportion (17%) among the alcohols. Surface and structural information concerning the activated catalysts, derived from X-ray diffraction, temperature-programmed reduction, Mössbauer, and photoelectron spectroscopy, revealed the appearance of a CoFe phase under the conditions employed during the catalyst activation. In the bimetallic cobalt–iron catalysts, this CoFe phase is suggested to be responsible for the rather high selectivity toward alcohol formation.

KEY WORDS: FT synthesis; Co and Fe catalysts; Mossbauer; alcohols; hydrocarbons.

1. Introduction

The conversion of natural gas to liquids (gas-to-liquids, GTL), and more specifically clean fuels and chemical feedstocks via Fischer–Tropsch technology, is currently of increasing interest. The catalytic synthesis of hydrocarbons from $CO + H_2$ mixtures leads to a large variety of products such as paraffins, olefins, alcohols and aldehydes, whose abundance depends on the catalysts employed and also on the operation conditions [1,2]. On scrutinizing the catalytic systems employed for the catalytic synthesis of hydrocarbons, it is clear that cobalt and iron are those most commonly used. Cobalt catalysts are suited for producing high yields of long-chain alkenes in FT synthesis. They are also characterized by a low ability to yield oxygenates and hence produce larger amounts of water than iron-based catalysts. Additionally, cobalt catalysts exhibit considerable stability in the metallic state and only a low tendency to form cobalt carbides. By contrast, iron catalysts display higher yields to oxygenated products [3], a lower selectivity to water as a consequence of the water-gas-shift reaction ($CO + H_2O \rightarrow CO_2 + H_2$), and the formation of surface iron carbides.

The incorporation of cobalt or iron phases in a support substrate results in substantial changes in both activity and product distributions. It has been shown that the acid-base and textural properties of supported catalysts play an important role in FT synthesis since the specific activity of methane formation tends to decrease with the increase in the pore size of the catalyst. In addition, the use of an inert support enhances C–C chain growth probability, and hydrocarbon formation would be favored by the presence of micropores since mass-transfer resistance is fairly low and residence time is improved [4].

In light of the above, the present work was undertaken with the aim of exploiting the beneficial effect of a silica support and the incorporation of both cobalt and iron species on performance for FT synthesis. In particular, emphasis is placed on the formation of CoFe intermetallics after catalyst activation and their role in oxygenate formation during the FT synthesis reaction in a fixed-bed microreactor. Some clues as to the nature of the chemical species developed on the silica-supported CoFe catalysts were revealed by X-ray diffraction (XRD), X-ray photoelectron spectroscopy (XPS), Mössbauer Spectroscopy and temperature-programmed reduction (TPR).

2. Experimental

2.1. Catalyst preparation

Silica-supported cobalt and iron catalysts were prepared by the wetness impregnation method on a

* To whom correspondence should be addressed.

1011-372X/03/0600–0123/0

silica carrier (Grace Davison, 310 m^2/g, 1.22 m^2/g) with cobalt nitrate $[Co(NO_3)_2]6H_2O$ and $[Fe(NO_3)_3]9H_2O$ aqueous solutions. Two bimetallic FeCo-supported catalysts containing a fixed amount of cobalt (10% Co) and different amounts of Fe (1% and 5% Fe), 1Fe10Co and 5Fe10Co, were prepared. For comparison, a reference silica-supported iron catalyst containing 10% Fe (10Fe) was also prepared. All impregnates were dried at 393 K overnight and calcined at 773 K under flowing air for 2 h.

2.2. Catalyst characterization

Specific areas of the catalysts were calculated by applying the BET method to the nitrogen adsorption isotherms, recorded on a Micromeritics Tristar 3100 device. Elemental analysis was performed by inductively coupled plasma emission spectroscopy (ICP-AES) (Perkin Elmer optima 3300 DV). X-ray diffraction patterns were recorded from calcined, reduced and used catalysts, using a Seifert 3000P diffractometer with nickel-filtered Ka radiation ($\lambda = 0.1538$ nm). For each sample, Bragg angles between 5 and 80° were scanned at a rate of 5 s per step (step size: 0.04° 2θ). Mössbauer spectra were recorded in sinusoidal mode, using a transmission spectrometer with a $^{57}Co/Rh$ source. Spectral analyses were performed by nonlinear fit, using the NORMOS [5] program, and energy calibrations were accomplished with α-Fe (6 μm) foil.

Temperature-programmed reduction (TPR) was carried out in a Micromeritics 3000 apparatus by flowing a 10% H_2/Ar mixture (50 cm^3/min) through the sample. Temperature was increased from 323 to 1073 K at a rate of 10 K/min and the amount of hydrogen consumed was determined with thermal conductivity detectors (TCDs). The effluent gas was passed through a cold trap placed before TCD in order to remove water from the exit stream of the reactor.

Photoelectron spectra (XPS) were acquired with a VG Escalab 200R spectrometer equipped with a hemispherical electron analyzer and AlKa (h.v = 1486.6 eV) X-ray source. The powder samples were mounted on a sample rod placed in a pretreatment chamber and degassed at 373 K for 1 h. Once the sample had been analyzed, it was moved back to the pretreatment chamber and reduced *in situ* under H_2 at 773 K or treated. Intensities were estimated by calculating the integral of each peak and fitting the experimental curves to Lorentzian/Gaussian lines. All binding energies (BEs) were referenced to the Si 2p line at 103.4 eV. Atomic ratios were computed from the intensity ratios normalized by atomic sensitivity factors [6].

2.3. Activity measurements

Activity tests were carried out using an automatic high-pressure fixed-bed catalytic reactor. The catalyst (0.30 g) was activated for 2 h in a mixture of $H_2/N_2 = 1:9$ (molar) at 773 K and atmospheric pressure. The reaction was accomplished at an overall pressure of 20 bar and temperatures of 493, 513 and 533 K. The composition of the feed stream—33.3% CO and 66.7% H_2—was adjusted by electronic mass flow controllers (Brookhorst). The system permitted on-line analysis of the effluent gas stream through a multiple gas chromatograph (GC) column system. A Hewlett-Packard 5890 gas chromatograph equipped with SPB-5 and PoraPlot Q capillary columns was used for product separation. Product analysis was carried out with thermal conductivity (TCD) and flame ionization (FID) detectors, which cover the analysis of CO, CO_2, and C_1-C_{20} hydrocarbons, and C_1-C_{10} alcohols.

3. Results and discussion

The chemical analyses obtained using ICP-AES are summarized in table 1. The data indicate that the measured metal loadings approach the nominal values expected from catalyst preparation. The BET specific areas and pore volumes of the fresh calcined catalysts and of the bare SiO_2 substrate are shown in table 2. Incorporation of cobalt and/or iron to the SiO_2 support led to a decrease in both BET areas and pore volumes. No apparent changes in these textural parameters were

Table 1
Elemental analysis for $CoFe/SiO_2$ system

	Elemental analysis			
	Metal loading (% Co)		Metal loading (% Fe)	
Catalyst	Theoretical	ICP	Theoretical	ICP
Co10	10	9.8	–	–
Fe10	–	–	10	9.5
CoFe10/5	10	8.6	5	4.6
CoFe10/1	10	9.4	1	–
Co10-2c	10	10.2	–	–
Fe10-c	–	–	10	10.2
CoFe10/5c	10	9.3	5	5.1
CoFe10/1c	10	9.4	1	0.9

Table 2
Textural parameters of the samples

	N_2 Adsorption	
Catalyst	S_{BET} (m^2/g)	V_{ads} ($P/P^0 = 0.98$) cm^3/g
SiO_2	289	1.19
SiO_2-c	300	1.18
Co10-c	219	0.80
Fe10-c	216	0.93
CoFe10/1-c	221	0.96
CoFe10/5-c	210	0.88

observed when both Co and Fe oxides were incorporated simultaneously.

The crystal structure of the supported cobalt and iron phases of the catalysts pretreated under different environments was revealed by X-ray diffraction. The monometallic Co10-c sample displays the diffraction lines of the Co_3O_4 spinel [7], whereas the other monometallic Fe10-c sample exhibits the pattern of hematite (Fe_2O_3) [8,9]. In the patterns of the bimetallic CoFe10/5-c and CoFe10/1-c samples, both phases can be seen although the lines of hematite are strongly overshadowed by that of the Co_3O_4 spinel [8,11]. Diffractograms of the catalysts activated under a hydrogen flow at 773 K were also recorded. The patterns of the monometallic Co10-c and Fe10-c samples reduced in H_2 (figure 1) exhibit the lines of metallic Co and Fe, respectively. However, the reduced bimetallic CoFe10/5-c sample shows not only the lines of Co° and Fe° but also the characteristic diffractions of a bimetallic CoFe phase. In the CoFe10/1-c sample, containing much less iron than the CoFe10/5-c counterpart, only the individual Co° and Fe° phases are observed, but in no case is the bimetallic CoFe phase apparent, presumably as a consequence of the development of very low crystal size particles. Nonetheless, it should be remembered that the chemical state of the atoms and the structure of the CoFe particles are inevitably affected by exposure of the reduced phases to the environment [11,12].

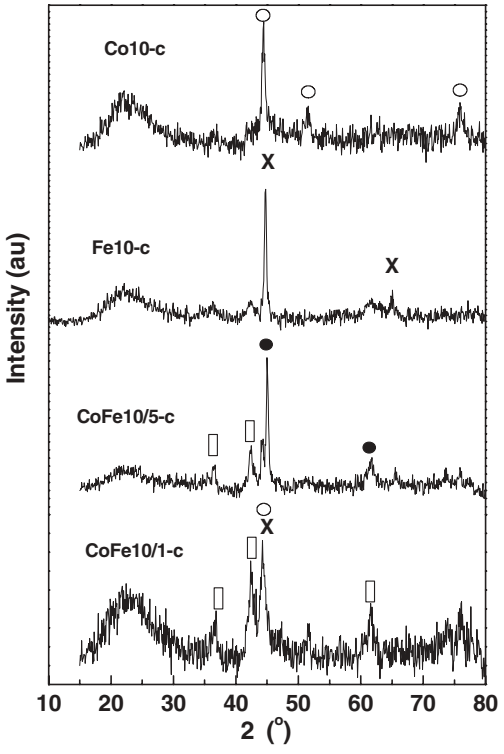

Figure 1. X-ray diffraction pattern of $Co/Fe(SiO_2)$ catalysts. Reduced in H_2 at 773 K. The crystalline phases identified are as follows: x, (Fe°); □, (CoO); ○, (Co°); and ●, (Fe/Co alloy).

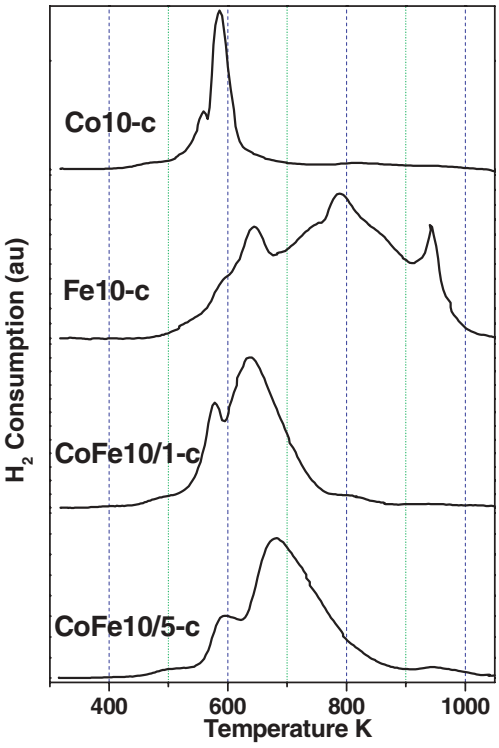

Figure 2. Temperature-programmed reduction profile of Co10-c, Fe10-c, CoFe10/1-c and CoFe10/5-c catalysts.

The activation of the catalysts in a hydrogen atmosphere was disclosed by TPR experiments. The TPR profiles of the catalysts are shown in figure 2. The TPR of the monometallic Co10-c sample exhibits a major peak at 586 K overlapped by a minor one at 563 K. In general, the reduction of cobalt oxide (Co_2O_3) proceeds through two consecutive reduction steps: $Co_2O_3 \rightarrow CoO \rightarrow Co°$. According to the stoichiometry of the two steps, the amount of H_2 consumed in the reduction of CoO species into Co° (peak at 586 K) would be double of that observed in the reduction of Co_2O_3 into CoO (peak at 563 K) [13]. Since the ratio of peak areas does not fit such a stoichiometry, it can be inferred that the starting cobalt oxide is close to the Co_3O_4 phase. This observation is consistent with the diffraction data, which only point to the presence of the Co_3O_4 phase in the calcined Co10-c sample. The TPR of the Fe10-c monometallic catalyst is more complex and exhibits three broad peaks at 644, 793 and 973 K. In agreement with previous observations, these peaks can tentatively be assigned to the following consecutive reduction steps [14]: α-$Fe_2O_3 \rightarrow Fe_3O_4 \rightarrow FeO \rightarrow Fe°$, although other effects—such as metal oxide dispersion and metal oxide–support interactions—would mask each of these steps. Figure 2 also shows the TPR profiles of the two CoFe10/5-c and CoFe10/1-c catalysts. These two profiles resemble that of the Co10-c sample, although the maxima of both peaks are shifted toward higher temperatures—more for the sample with the lower amount of iron (CoFe10/1-c)—and become broader. Both findings should also be taken as indicating the

interaction between cobalt and iron oxides in the calcined state.

The chemical state of the elements and their relative abundances on the catalyst surface were revealed by photoelectron spectroscopy. The binding energies of core electrons and surface atomic ratios of cobalt and/or iron relative to silicon are summarized in table 3. The calcined Co10-c sample shows two components for the $Co2p_{3/2}$ core level: one at 779.6 eV, associated with Co^{3+} in octahedral positions, and another at 781.5 eV, assigned to Co^{2+} in tetrahedral positions of the Co_3O_4 spinel [15]. Upon H_2 reduction, the spinel structure collapses, as illustrated by the dramatic change seen in the line profiles and peak components: one peak at 779.7 eV points to the presence of octahedral Co^{3+} ions, presumably in the nondecomposed Co_3O_4 phase, and two new peaks at 777.7 and 781.9 eV, assigned to Co° and octahedral Co^{2+} ions, respectively. The Fe $2p_{3/2}$ peak of the Fe10-c sample exhibits two components at binding energies of 709.6 and 711.0 eV. These components can be ascribed to Fe^{2+} and Fe^{3+} species, respectively. The reduced sample displays a similar profile, except that a fraction of Fe^{3+} (711.0 eV) is reduced to Fe^{2+} (709.4 eV) (table 3). The two bimetallic (CoFe10/5-c and CoFe10/1-c) catalysts display similar Co2p and Fe profiles, although iron is more easily reduced than in the monometallic Fe10-c [16] and cobalt reduction is slightly inhibited. This observation agrees with the findings reported in the literature [17] and is consistent with the above TPR data.

Table 3
Binding energies of core electrons and surface atomic ratios of the catalysts (In brackets, percentage of oxidation states)

Sample		Co $2p_{3/2}$	Fe $2p_{3/2}$	Co/Si at	Fe/Si at
Co10-c	Vacuum	779.6 (70) 781.5 (30)	– –	1.5	–
	Reduced	777.7 (35) 779.7 (41) 781.9 (24)	– – –	1.98	–
Fe10-c	Vacuum	– –	709.6 (58) 711 (42)	– –	0.97 1.03
	Reduced	– –	711 (65) 709.5 (35)		
CoFe10/1-c	Vacuum	779.7 (67) 781.7 (33)	709 (47) 711 (53)	2.08	0.46
	Reduced	777.9 (17) 779.9 (58) 781.9 (26)	707.3 (19) 709.4 (44) 711.2 (37)	1.94	0.49
CoFe10/5-c	Vacuum	779.8 (70) 781.7 (30)	709.4 (41) 711.2 (59)	1.59	0.88
	Reduced	777.9 (19) 779.9 (48) 781.9 (32)	707.3 (7) 711.1 (63) 709.3 (30)	2.55	2.24

Mössbauer spectra of two representative Fe-containing samples are shown in figure 3. The Mössbauer spectrum of the reduced Fe10-c sample is compared with that of the calcined counterpart in figure 3(A). Similarly, the spectrum of the reduced CoFe10/5-c sample is compared with that of the calcined counterpart in figure 3(B). The Fe in unreduced Fe10-c and CoFe10/5-c is present as Fe^{3+} in the form of α-Fe_2O_3. The small magnetic field (50.4(1)T) of the hematite is due to the

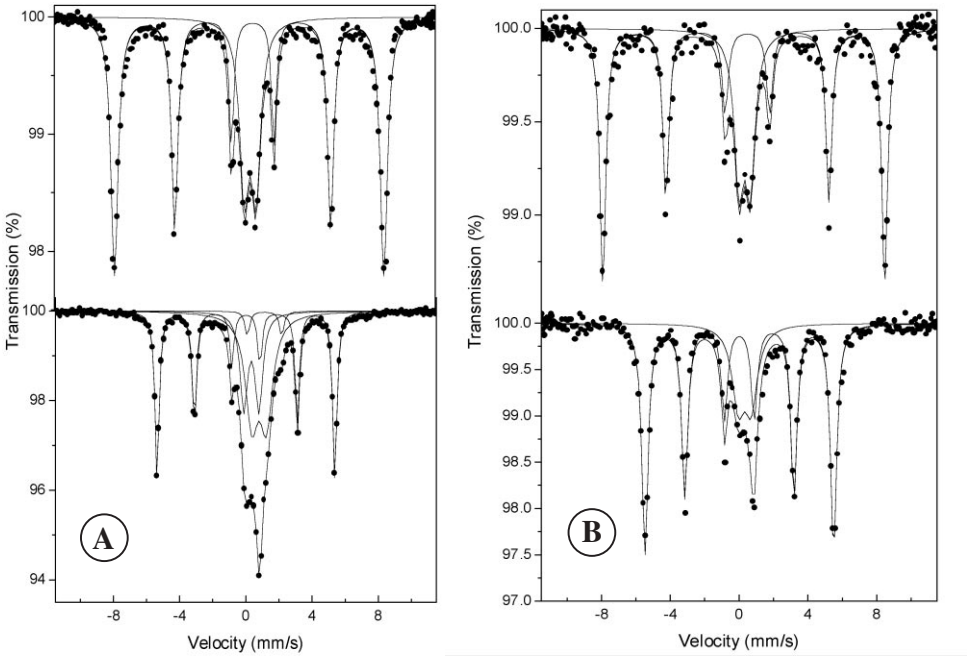

Figure 3. Mössbauer spectra of unreduced (up) and reduced (down) in H_2 at 773 K. (A) Fe10-c; and (B) CoFe10/5-c catalysts.

Table 4
Mössbauer hyperfine parameters

Catalyst		Components	δ (mm/s)	QS (m/s)	H_{hf} (T)	%
Fe10-c	Unreduced	α-Fe_2O_3	0.37	0.21	50.4	71
		α-Fe_2O_3	0.33	0.71		29
	Reduced	α-Fe	0.00	0.01	33.2	39
		α-Fe_2O_3	0.33	0.92		20
		$Fe_{1-x}O$	0.79	0.87		38
		Fe^{2+}	1.12	2.07		3
CoFe10/5-c	Unreduced	α-Fe_2O_3	0.37	0.21	50.7	69
		α-Fe_2O_3	0.32	0.65		31
	Reduced	CoFe	0.01	0.01	33.9	76
		α-Fe_2O_3	0.33	0.74		24

small particle size [18]. The presence of a superparamagnetic doublet also reveals the existence of nanometer-sized particles. The Mössbauer hyperfine parameters and their assignment are offered in table 4. The reduction of both systems under the working conditions gives different results (figure 3(B) and table 4). Nearly 80% of α-Fe_2O_3 in both samples is reduced, under the assumption of an equal recoilless fraction for all compounds. The Mössbauer spectrum of the reduced monometallic Fe10-c arises from the convolution of a sextet of α-Fe and several doublets of Fe^{2+} species. Along the reduction, 38% of the metastable $Fe_{1-x}O$ phase (wurzitte) and a very small amount of an Fe^{2+} oxyhydroxide were developed. The parameters of these species are given in table 4. By contrast, the Mössbauer spectrum of the reduced CoFe10/5-c sample points to the appearance of the CoFe [19] alloy, although the $Fe_{1-x}O$ species were absent.

Activity data of the catalysts used in the FT reaction are shown in table 5. The monometallic Co10-c catalyst shows a moderate CO conversion and low selectivity to alcohols, while the yield of C_{5+} hydrocarbons is quite high. However, the monometallic Fe10-c catalyst displays a higher selectivity to alcohols, with a slight drop in the hydrocarbon yield and an apparent increase in the lighter fraction. The results on activity for the bimetallic CoFe10/5-c sample are similar, although the increase in temperature led to a significant drop in the rate of methane formation and a simultaneous increase in yield to liquid hydrocarbons. Furthermore, selectivity to alcohols increased with respect to the monometallic Co10-c, and this was moderately high (15% to C_{3+}OH alcohols), while the selectivity of the longer carbon chain proved to be higher than that of the monometallic Fe10-c. Finally, the bimetallic CoFe10/1-c catalyst showed an increase in methane selectivity (31%), which was compensated by a drop in the selectivity to C_{5+} hydrocarbons. Selectivity to alcohols was fairly high (29%), and ethanol reached the highest proportion (17%) among the alcohols.

4. Conclusions

Activity and product distribution along the hydrogenation of CO on silica-supported cobalt–iron catalysts was found to depend strongly on the catalysts' composition. The Fe-free catalyst exhibited fairly high selectivity (67%) toward C_{5+} formation and a low methanation rate, while in its Co-free counterpart the lower C_{5+} fraction was compensated by an increase in the formation of lighter hydrocarbon fractions and alcohols. The bimetallic CoFe catalysts proved to be much more attractive in terms of alcohol formation. In the bimetallic CoFe10/5-c catalyst, selectivity to alcohols increased with respect to the monometallic Co10-c, and this was moderately high (15% to C_{3+}OH alcohols). An even better selectivity to alcohols was found for the

Table 5
CO conversion and product distributions on the catalysts

		% Selectivity							
Catalyst	% Conversion	C_1	C_2	C_3	C_4	C_{5+}	MeOH	EtOH	C_{3+}OH
Co10-c	3.5	10	4	8	7	67	0.3	1.7	2.7
Fe10-c	12.5	15	9	16	8	41	2	2	5
CoFe10/5-c	12.3	19	10	15	8	28	4	1	15
CoFe10/1-c	6.9	31	7	10	4	19	5	17	7

Reaction conditions: 513 K, 2 MPa, $H_2/CO = 2$, GHSV= 800 h^{-1}.

bimetallic CoFe10/1-c sample, where selectivity to alcohols was quite high (29%), and ethanol reached the highest proportion (17%) among the alcohols.

Under the conditions employed during catalyst activation, the surface and structural data obtained by XRD, TPR, and Mössbauer and photoelectron spectroscopy pointed to the formation of a CoFe phase. In the bimetallic cobalt–iron catalysts, this CoFe phase appears to be responsible for the rather high selectivity toward alcohol formation.

Acknowledgments

A fellowship (V.P.O.) granted by the Repsol-YPF Foundation is acknowledged. This work was partly supported by MCYT (Spain) through the Project MAT2001-2215-C03-01.

References

[1] M.E. Dry, in *The Sasol Fischer-Tropsch Processes*, B. Leach (ed.), App. Industrial Catal., Chapter 5, (Academic Press, New York, 1983).
[2] W.O. Haag, J.C. Kuo and I. Weller. Gasification for synthesis of fuels and chemicals, Chapter V, *Coal Gasification, Direct Application and Synthesis of Chemical and Fuels*, (1987) pp. 117–205.
[3] H. Schulz, Appl. Catal. A: Gen. 186 (1999) 3–12.
[4] B. Ernst, S. Libs, P. Chaumette and A. Kiennemann, Appl. Catal. A: Gen. 186 (1999) 145–168.
[5] R.A. Brand, Nucl. Instrum. Methods Phys. Res., Sect. B 28 (1987) 398.
[6] C.D. Wagner, L.E. Davis, M.V. Zeller, J.A. Taylor, R.H. Raymond and L.H. Gale, Surf. Interface Anal. 3 (1981) 211.
[7] B.K. Sharma, M.P. Sharma, S. Kumar, S.K. Roy, S. Badrinarayanan, S.R. Sainkar, A.B. Mandale and S.K. Date, Appl. Catal. A: Gen. 211 (2001) 203–211.
[8] F.P. Larkins and A.Z. Khan, Appl. Catal. 47 (1989) 209–221.
[9] K. Jthimurugesan, J.G. Goodwin Jr., K. Santosh, K. Ganwal and J.J. Spivey, Catal. Today 58 (2000) 355–344.
[10] D.S. Kalakkad., M.D. Shroff, S. Köhler, N. Jackson and A.K. Datye, Appl. Catal. A: Gen. 133 (1995) 335–350.
[11] D.J. Duvenhage and N.J. Coville, Appl. Catal. A: Gen. 153 (1997) 43–47.
[12] J.A. Amelse, L.H. Schwartz and J.B. Butt, J. Catal. 72 (1981) 95.
[13] M.P. Rosynek and C.A. Polansky, Appl. Catal. A: Gen. 73 (1991) 97–112.
[14] R. Brown, M.E. Cooper and D.A. Whan, Appl. Catal. 3 (1982) 177.
[15] B. Ernst, A. Bensaddik, L. Hilaire, P. Chaumette and A. Kiennemann, Catal. Today 39 (1998) 329–341.
[16] D.D. Hawnm and B.M. Dekoven, Surf. Interface Anal. 10 (1987) 63.
[17] D.J. Duvenhage and N.J. Coville, Appl. Catal. A: Gen. 233 (2002) 63–75.
[18] L.H. Bowen, Mössbauer Effect Ref. Data J. 2 (1979) 76.
[19] M. Sorescu and A. Grabias, Intermetallics 10 (2002) 317.